

Effect of Zn-Incorporation into $\text{Li}_7\text{La}_3\text{Zr}_2\text{O}_{12}$ Solid Electrolyte on Structural Stability and Electrical Conductivity: First-Principles Study

Xinghua Liang^{1,2,*}, Xinqi Li¹, Xi Wu¹, Qixin Gai¹, Xiaofeng Zhang^{2,*}

¹ Guangxi Key Laboratory of Automobile Components and Vehicle Technology, Guangxi University of Science & Technology, Liuzhou 545006, People's Republic of China

² National Engineering Laboratory for Modern Materials Surface Engineering Technology, Guangdong Institute of New Materials, Guangdong Academy of Science, Guangzhou 510650, People's Republic of China

*E-mail: lxh304@aliyun.com, zxf200808@126.com

Received: 5 June 2020 / Accepted: 24 July 2020 / Published: 30 September 2020

The electronic structures of Zn doped tetragonal $\text{Li}_7\text{La}_3\text{Zr}_2\text{O}_{12}$ at different locations are studied by using the first principles method based on DFT, and the structure optimization, energy band, density of states and population analysis are carried out. Results show that the mixed system of total energy is reduced, the structure is more stable, and Li doping of total energy of -53104eV, more stability. Due to the effect of electrons in different orbitals of Zn, the band number near Fermi level increases, the band gap decreases, the energy required for electron or hole transition decreases, and the conductivity increases. The band gap of La site doping is 3eV, and the conductivity is relatively high. Population analysis proves that the Zn-O bond length of the $\text{Li}_6\text{ZnLa}_3\text{Zr}_2\text{O}_{12}$ system is 1.947Å, which is shorter than the $\text{Li}_7\text{La}_2\text{ZnZr}_2\text{O}_{12}$ system and has better stability. In addition, the length of the Li-Li bond in the doped system is shortened, and the Coulomb repulsion force between Li^+ and Li^+ is increased, which is conducive to increasing the concentration of Li vacancies, thereby improving the conductivity. Although doping can improve stability and conductivity, the amount of doping is too large, which is not conducive to improving the conductivity.

Keywords: $\text{Li}_7\text{La}_3\text{Zr}_2\text{O}_{12}$, Zn-incorporation, Electronic structure, First-principles

1. INTRODUCTION

Solid state lithium ion battery has the advantages of high safety performance high energy density and wide operating temperature range, so it is a research hotspot in the field of lithium ion battery [1]. Garnet-type LLZO structure has become the main research object of electrolyte materials for all solid state lithium-ion battery because of its higher ionic conductivity, good chemical and

electrochemical stability, wide electrochemical window and strong compatibility with metal lithium [2-3]. Studies have shown that $\text{Li}_7\text{La}_3\text{Zr}_2\text{O}_{12}$ with cubic and square phase crystal structure, Li^+ occupies different positions in the two structures. The tetragonal structure ($I41/acd$) has a lower concentration of Li^+ vacancies, which results in low ionic conductivity; the ionic conductivity of cubic ($Ia3d$) is relatively high but unstable under normal temperature conditions [4-7]. Therefore, in-depth research on the preparation process and mechanism of LLZO materials, and exploring the reasons for the differences in the conductivity and stability of different crystal structures, are of great significance for improving the conductivity and chemical properties of materials.

First-principles calculations are commonly used calculation methods to study the microstructure and properties of substances. Bernstein [8] and Adams [9] studied the Li^+ distribution of $\text{Li}_7\text{La}_3\text{Zr}_2\text{O}_{12}$ materials and the relationship between temperature and phase transition by first principles. It is found that Li^+ is arranged differently in different phases. Increasing the concentration of lithium vacancy can decrease the temperature of phase transition. Experiments have proven that the temperature is lowest when the lithium content is around 6.5 [10]. Xu [11] calculated the $\text{Li}_x\text{La}_3\text{M}_2\text{O}_{12}$ system to show that Li^+ transitions in the octahedral-octahedral mode when $x=5$, and Li^+ tends to transition in the octahedral-tetrahedral-octahedral mode when $x=7$. Wang [12] also confirmed the Li^+ transition mode at $x=5$. Adams [9] thought that the transition between Li^+ between octahedra would be hindered by the tetrahedron occupation, and the tetrahedral vacancies could be increased by higher valence doping to improve the conductivity. Geiger [13] found that doping Al^{3+} at the Li^+ site can stabilize LLZO and improve the conductivity, and determined the doping mode at the Li^+ site by calculation [14]. Miara [15] calculated the doping of different elements and found that lowering the unit cell parameters will reduce the conductivity, and it is related to the Li^+ vacancy and concentration. Experiments also prove that elemental doping can change the concentration of Li^+ vacancies and improve the conductivity. Li Guangzong [16] studied the effect of Zn doped Li sites on the conductivity of LLZO materials. When the Zn concentration was 0.2, the conductivity of the material reached $1.20 \times 10^{-3} \text{ S / cm}$. Ohata [17] reported that the position where Nb replaced Zr can increase the vacancy concentration of Li, and the conductivity of the material reached $8 \times 10^{-4} \text{ S / cm}$ at room temperature. In addition, doping elements such as Te, Y, Sb, Ta, Sr, and In to the Zr^{4+} site can also improve the conductivity [10, 18-21]. Under the same mechanism, doping La site [22, 23], co-doping Li site with Zr site or Li site with La site [14, 24] can also improve structural stability and electrical conductivity.

Because the higher conductivity of LLZO cubic phase structure, which is favored by researchers, the research on the calculation and modification of tetragonal phase structure is relatively insufficient. Based on this research, the first-principles ultra-soft pseudo-potential plane wave method is used to calculate the tetragonal LLZO model and the Zn-doped Li-site and La-site models. Analyze and compare the band structure, atomic layout, and states of the three models. The change of electronic structure such as density, the effects of Zn doping and different doping positions on the electronic structure and properties of $\text{Li}_7\text{La}_3\text{Zr}_2\text{O}_{12}$ were discussed, which provided a theoretical basis for the modification of $\text{Li}_7\text{La}_3\text{Zr}_2\text{O}_{12}$ solid electrolyte.

2. STRUCTURE AND COMPUTATION METHOD

2.1 Structure model

$\text{Li}_7\text{La}_3\text{Zr}_2\text{O}_{12}$ has two crystal structures. The tetragonal structure space group is $I41/acd$, which the lattice constants are $a=13.134\text{\AA}$, $c=12.663\text{\AA}$, and $c/a=0.9641$ [4, 25]. The crystal structure frame is composed of hexahedron $[\text{LaO}_8]$ and octahedron $[\text{ZrO}_6]$, Li^+ occupies three positions of 8a of tetrahedron and 16f, 32g of octahedron, the occupancy rate is 1 at octahedron position, but it is empty at 16e of tetrahedron [5, 6, 26].

The unit cell structure is symmetrical and periodic. The tetragonal LLZO supercell structure was obtained using the ICSD database. Due to the large number of atoms, in order to reduce the amount of calculation and calculation time, the supercell was changed to the primitive cell according to the principle of symmetry. The substitution is performed to generate calculation models of Zn doping at different positions: $\text{Li}_6\text{ZnLa}_3\text{Zr}_2\text{O}_{12}$ and $\text{Li}_7\text{La}_2\text{ZnZr}_2\text{O}_{12}$, and optimization calculations are performed for the undoped and doped models. Figure1 (a ~ c) shows three calculation models of primitive cells.

2.2 Computational details

The structure optimization, energy band and density of states of the model are calculated by using the CASTEP module of MS software and the platform of Shenzhen Cloud Computing Center. In the calculation, the generalized gradient approximation (GGA) PBE functional method was used to correct the exchange correlation potential of the electron-electron interaction. All elements are calculated by ultra-soft pseudopotential plane method. The valence electrons selected for atomic pseudo-potential calculation were $\text{Li } 1s^2 2s^1$, $\text{O } 2s^2 2p^4$, $\text{Zn } 3d^{10} 4s^2$, $\text{Zr } 4s^2 4p^6 4d^2 5s^2$ and $\text{La } 5s^2 5p^6 5d^1 6s^2$.

Through a large number of analysis calculations, the structural optimization calculation accuracy is set to fine, the truncated kinetic energy is 340eV, and the Brillouin area is calculated using a $4\times 4\times 4$ k-point grid. The convergence criterion is: the total energy difference convergence threshold $dE/ion = 1.0\times 10^{-5}\text{eV}$, force convergence threshold $|F|_{max}=0.3\text{eV/\AA}$, displacement convergence threshold $|dR|_{max}=1.0\times 10^{-3}\text{\AA}$, stress component convergence threshold $|S|_{max}=5.0\times 10^{-2}\text{GPa}$. Set the truncated kinetic energy for the calculation of kinetic energy to 500eV and adopt $5\times 5\times 5$ k-point grid. What's more, set the convergence accuracy to $2.0\times 10^{-6}\text{eV}$.

Because the LLZO crystal structure contains more elements, and each atom occupies a different position in the space structure, this has certain effects on determining the doping position and calculating analysis. Therefore, before determining the doping position, select different atom positions in the La position for doping calculation. A large number of calculations show that the total energy difference obtained by doping at different positions is within 0.2eV. In order to reduce the amount of calculation and ignore the effect of atomic positions, the $\text{Li}_6\text{ZnLa}_3\text{Zr}_2\text{O}_{12}$ model was replaced by replacing four Li with (0.75, 0.25, 0.5) positions according to symmetry. Similarly, the $\text{Li}_7\text{La}_2\text{ZnZr}_2\text{O}_{12}$ model was replaced by (0.25, 0.25, 1) positions.

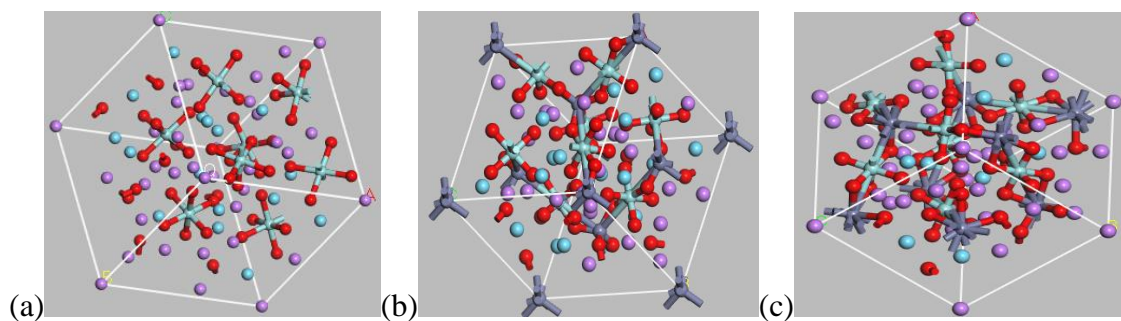


Figure 1. (a) $\text{Li}_7\text{La}_3\text{Zr}_2\text{O}_{12}$ calculation model. (b) $\text{Li}_6\text{ZnLa}_3\text{Zr}_2\text{O}_{12}$ calculation model. (c) $\text{Li}_7\text{La}_2\text{ZnZr}_2\text{O}_{12}$ calculation model.

3. RESULTS AND DISCUSSION

3.1 Structure optimization and total energy

According to the principle of minimum total energy, the three models are optimized to obtain the total energy and lattice parameters. As shown in Table 1, $a=b \neq c$ and $\alpha=\beta=\gamma=90^\circ$, which is consistent with the lattice parameters reported in reference [25]. Compared with the initial values ($a=13.134\text{\AA}$, $c=12.663\text{\AA}$), the volume increases to 1138.34\AA^3 with the increase of lattice constant. But the error is 1.68%, which shows that the establishment of the model is correct and reliable within the range allowed by the pseudopotential plane wave method. In addition, the Li site doping leads to the original cell size is 1162.95\AA^3 , and the total energy reaches the lowest value -53104eV . And La doping contribute to the original cell volume of 1107.48\AA^3 , the total energy is on the decline. The decrease of the system energy indicates that the stability of the crystal structure is improved. The structure of the material is not easy to be destroyed during the lithium ion insertion and extraction process, it shows high cycle stability and life [27, 28]. Therefore, the doping of Zn at the Li site or the La site can improve the stability of the LLZO structure, and the Li site doping stability is better, which is consistent with the literature report [29]. However, doping at different positions results in different lattice constants, which may be related to the crystal structure, doping concentration and doping position.

Table 1. Lattice parameters and energy

| Model | a(\AA) | b(\AA) | c(\AA) | α ($^\circ$) | β ($^\circ$) | γ ($^\circ$) | Total Energy (eV) |
|--|-------------------|-------------------|-------------------|-----------------------|----------------------|-----------------------|-------------------|
| $\text{Li}_7\text{La}_3\text{Zr}_2\text{O}_{12}$ | 13.355 | 13.355 | 12.763 | 90 | 90 | 90 | -47039 |
| $\text{Li}_6\text{ZnLa}_3\text{Zr}_2\text{O}_{12}$ | 13.511 | 13.511 | 12.739 | 90 | 90 | 90 | -53104 |
| $\text{Li}_7\text{La}_2\text{ZnZr}_2\text{O}_{12}$ | 13.191 | 13.191 | 12.727 | 90 | 90 | 90 | -50396 |

3.2 Energy band and density of states analysis

According to the calculation, the energy bands and total density of states of different models are obtained, as shown in Fig. 2(a~c) and Fig. 3(d~f). Fermi level is taken as the energy zero, and the relevant data records of different energy bands near the Fermi level are recorded in Table 2.

According to the above figure and Table 2, the $\text{Li}_7\text{La}_3\text{Zr}_2\text{O}_{12}$ energy band (a) is mainly distributed between $-47\sim 25\text{eV}$, with a large part of the bandwidth and overlapping between adjacent tracks.

Table 2. Energy band parameters of different models

| Structure | Range (eV) | Conduction band (eV) | Valence band (eV) | Band gap (eV) |
|--|---------------------|----------------------|--------------------|---------------|
| $\text{Li}_7\text{La}_3\text{Zr}_2\text{O}_{12}$ | $-46.89 \sim 24.73$ | $3.96 \sim 24.73$ | $-3.37 \sim 0$ | 3.96 |
| $\text{Li}_6\text{ZnLa}_3\text{Zr}_2\text{O}_{12}$ | $-47.00 \sim 24.20$ | $-0.41 \sim 21.68$ | $-9.13 \sim -4.22$ | 3.81 |
| $\text{Li}_7\text{La}_2\text{ZnZr}_2\text{O}_{12}$ | $-51.16 \sim 21.68$ | $3.07 \sim 24.17$ | $-5.01 \sim 0.07$ | 3.00 |

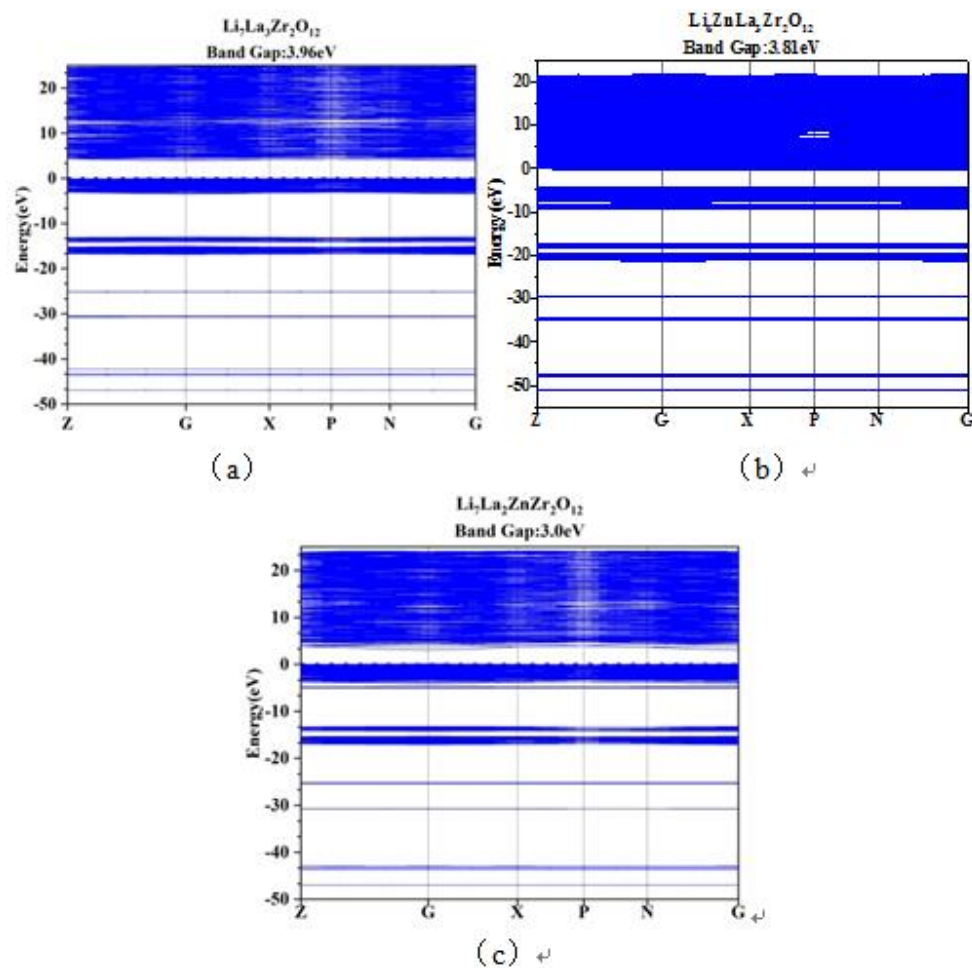


Figure 2. Energy band diagrams of three models

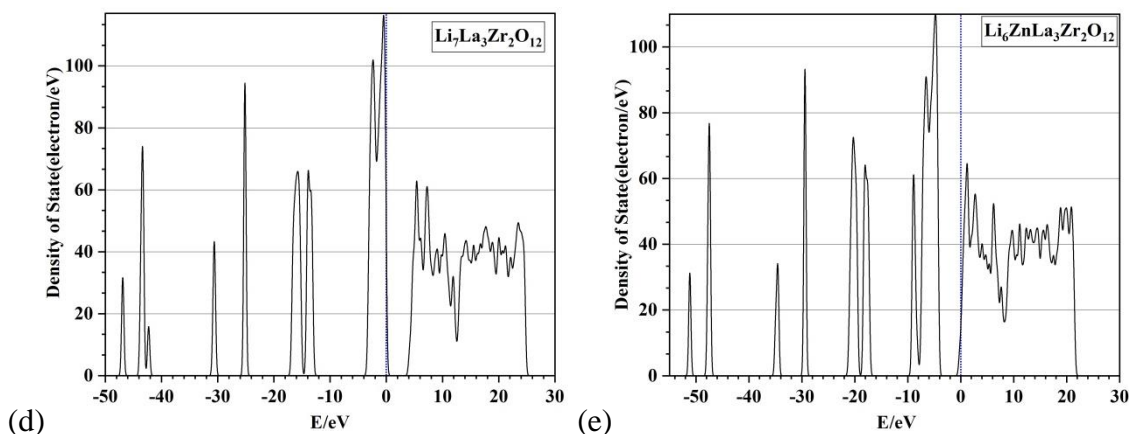
The conduction bandwidth is 20.77eV , the valence bandwidth is 3.37eV . Bottom point of the guide belt and vertex of valence band are at the same high symmetry point G, so the $\text{Li}_7\text{La}_3\text{Zr}_2\text{O}_{12}$ crystal has a direct band gap. In addition, the band gap is large at 3.96eV and Fermi level is at the top of the valence band, which is similar to a p-type semiconductor material. So conductivity is determined by a small number of hole carriers, it also shows that the Li^+ is arranged in order in the tetragonal phase structure [30]. After doping, the energy band (b) as a whole moves to a lower energy direction, the band gap is reduced to 3.81eV . Guide band bottom passes through the Fermi level and the energy

required for electron transition is reduced. Compared with p-type semiconductors, the electrical conductivity increases. The structure of the energy band (c) is basically the same as that of the (a), Fermi level located in the valence band. Therefore valence band becomes the dissatisfied band, which the hole carrier concentration was increased. Compared with (a) and (b), the band gap is the lowest and the electrical conductivity is the highest. Similar to the results reported in literature [29, 31, 32], the conductivity of LLZO can be improved by doping, and the effects of doping at different positions are different.

The density of states diagram corresponds to the energy band diagram, and different energy bands occupy different intervals in the density of states diagram. According to the total density of states and energy band analysis, the density of states before and after doping is basically the same, but the peak intensity and position of different doping positions are different. The Fermi level is located at the point where DOS is close to 0 but not zero. The conduction band region on the Fermi level has a wider and uniform distribution, with lower peaks. The atomic orbital of the band is highly expandable. In addition, a peak position is added at -8.90eV in the Figure (e), with a peak value of 61.10eV, and a peak position is added at -15.85eV in the Figure (f), with a peak value of 70.19eV, which is due to the addition of the electronic orbital of Zn. Caused by changes in the electronic structure. After cationic doping, the arrangement of lithium ions in the crystal structure and the size of the migration channel are changed, which is beneficial to the improvement of structural stability and electrical conductivity [17, 33]. In addition, the pseudo-energy gap of different state density is shown in Table 3, and the pseudo-energy gap of the doping system increases, indicating that the covalency of bonding in the system is enhanced. But the increase is small, indicating that the effect of doping at different locations is similar.

Table 3. Chirped energy gaps of different structures

| Model | Pseudo energy gap (eV) |
|--|------------------------|
| $\text{Li}_7\text{La}_3\text{Zr}_2\text{O}_{12}$ | 5.89 |
| $\text{Li}_6\text{ZnLa}_3\text{Zr}_2\text{O}_{12}$ | 5.97 |
| $\text{Li}_7\text{LaZnZr}_2\text{O}_{12}$ | 5.98 |



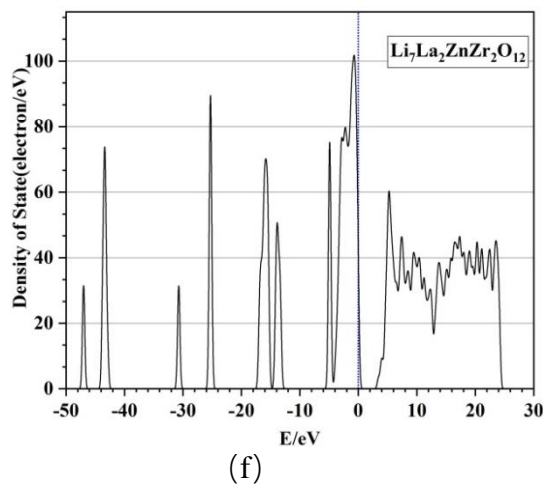


Figure 3. Total density of three models

For further analyze the relationship between electron orbitals and energy bands and densities of states of different atoms, the densities of states of different doping systems and elements are obtained, as shown in Figs.4 (1 ~ 5), 5 (6 ~ 11) and 6 (12 ~ 17).

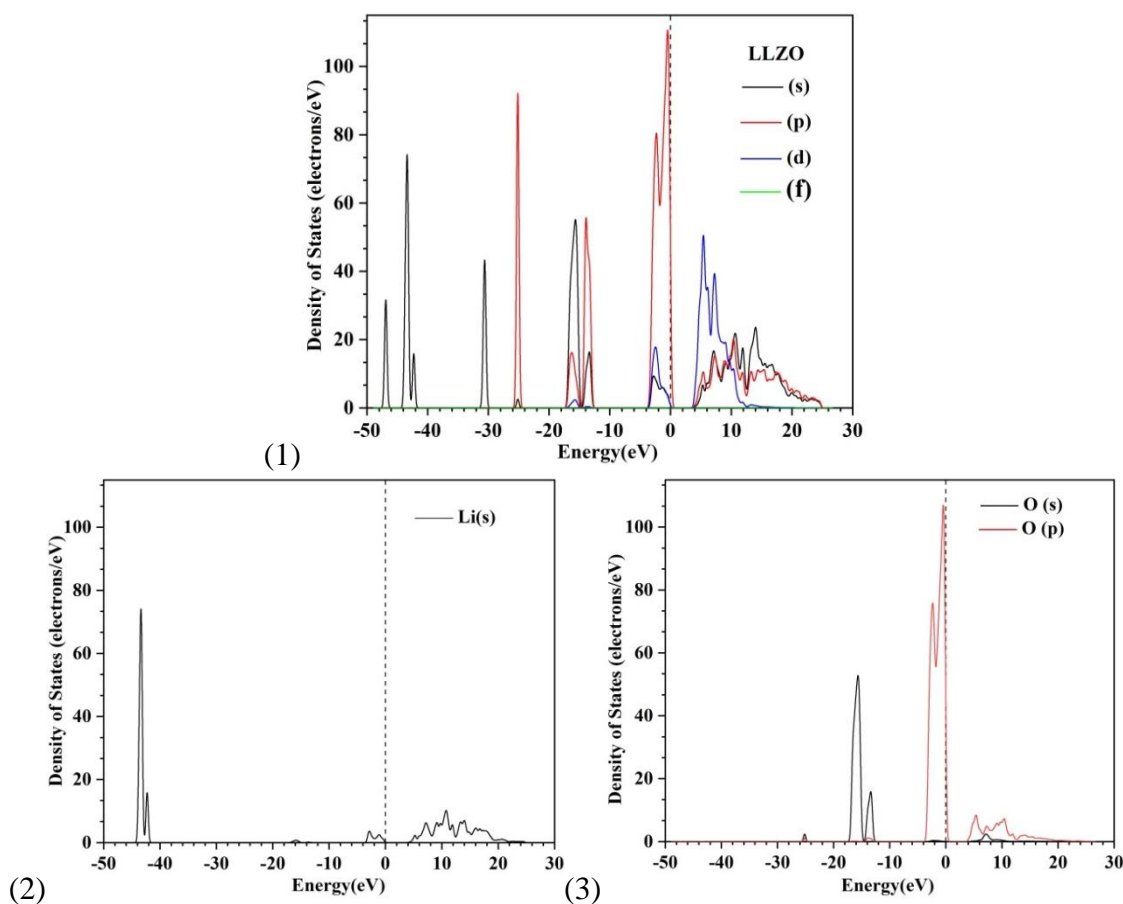
It can be seen from Fig.4 that the energy bands at -16.83 to -13.04 eV below the LLZO valence band are mainly Li, O s-orbitals, La p, d orbitals, and Zr p-orbitals, indicating that there is a strong common between the atoms Price key. The energy band generated at the energy level of -25.15 eV is the function of the O s-orbit and the Zr p-orbit, but the covalent bond between the two orbits is weak. The energy band generated at -30.62 eV is the Las orbital action, the energy band at $-44.56 \sim -41.37$ eV is the Li s-orbital action, and the energy band generated at -46.89 eV is the Zr s-orbital action. There is no overlap between the orbitals. In addition, the state density peaks of each energy band under the upper valence band are strong and the width is small, indicating that the locality is strong. The upper valence band near the Fermi level is the combined action of the Li s-orbits, O p-orbits, and the p and d orbits of La and Zr. Among them, there are two strong density peaks at -2.33 eV and -0.46 eV, which are mainly contributed by O 2p-orbital, La 5d-orbital, and Zr 4d-orbital. O, La, and Zr interact strongly. But in the conduction band, it shows strong delocalization, each atom's electron orbit contributes, and two more apparent density peaks are formed, which are contributed by La 5d and Zr 4d orbit electrons. There is overlap between the electron orbits of different atoms, and the interaction between Zr-O and La-O is strong, which is consistent with the skeleton structure of LLZO crystal [6, 25].

As can be seen from Fig.5 that compared with undoped Zn doping with Li site leads to the shift of energy band to low energy direction and the change of electronic structure. The partial density of states of La and Zr decreases as a whole, the density of p-orbital states of O decreases obviously, and the energy band is added at -8.94 eV. The energy band at the low energy level -42.29 eV in LLZO, which is contributed by the s-orbital of Li, disappears after the doping of Zn, but the energy band produced by the action of 4p and 3d orbitals of Zn is added to the forbidden band -8.89 eV at the bottom of the upper valence band. It interacts with Li s-orbitals, O p-orbitals and p and d orbitals of La and Zr to form a new valence band, the energy order increases, the valence band widens, and the generation of Zn-O interaction is beneficial to improve the structural stability. Due to the s, p, and d orbital effects of

Zn, the number of conduction bands also increases, the Fermi level enters the conduction band, the band gap decreases, the electrons transition more easily, and the conductivity is improved.

It can be seen from Fig. 6 that the p-orbital state density of O is the lowest, and the energy band generated by the 4p and 3d orbital action of Zn is added at the forbidden band at the bottom of the upper valence band -8.89eV. Its state density is the highest and the orbital overlap decreases. Zn-O interaction is reduced compared to Li-site doping. Compared with Fig.4, the number of valence bands increases due to the action of p and d orbitals of Zn, and the valence band is the widest at this time. The Fermi level is located in the valence band, and the band gap is the smallest. The energy level closer to the Fermi level is more likely to be occupied by free holes, and the hole carrier concentration increases, which is beneficial to improve the electrical conductivity.

According to the analysis of the energy band and the density of states, it is known that the electronic structure changes due to the electronic orbital action of the doping element. Doping Zn at the Li or La sites will increase the conductivity of the material, and the La site doping effect is more significant. Increasing the electrical conductivity of the material not only improves the electrochemical performance of the material, but also raises the content and cycle function of solid-state lithium battery [27, 34].



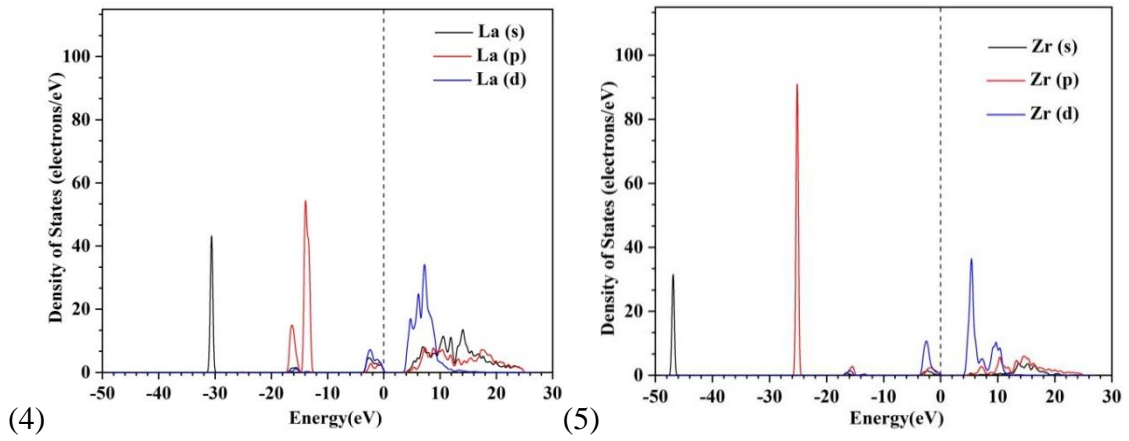
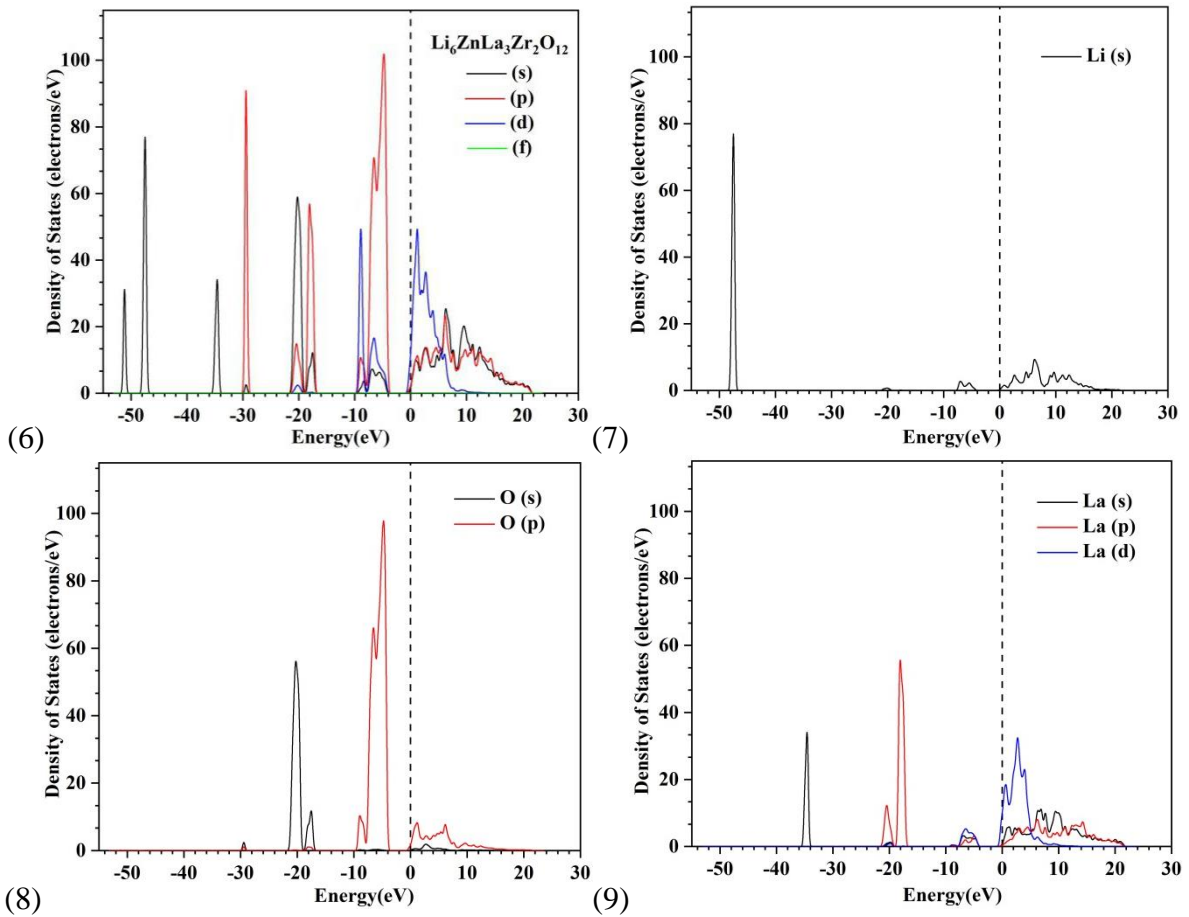


Figure 4. LLZO and the density of states of each atom



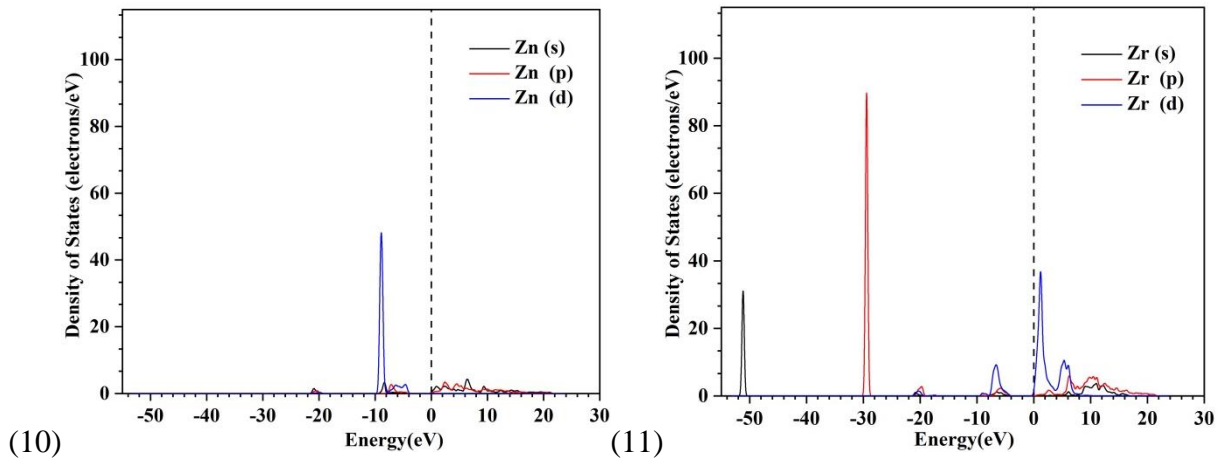
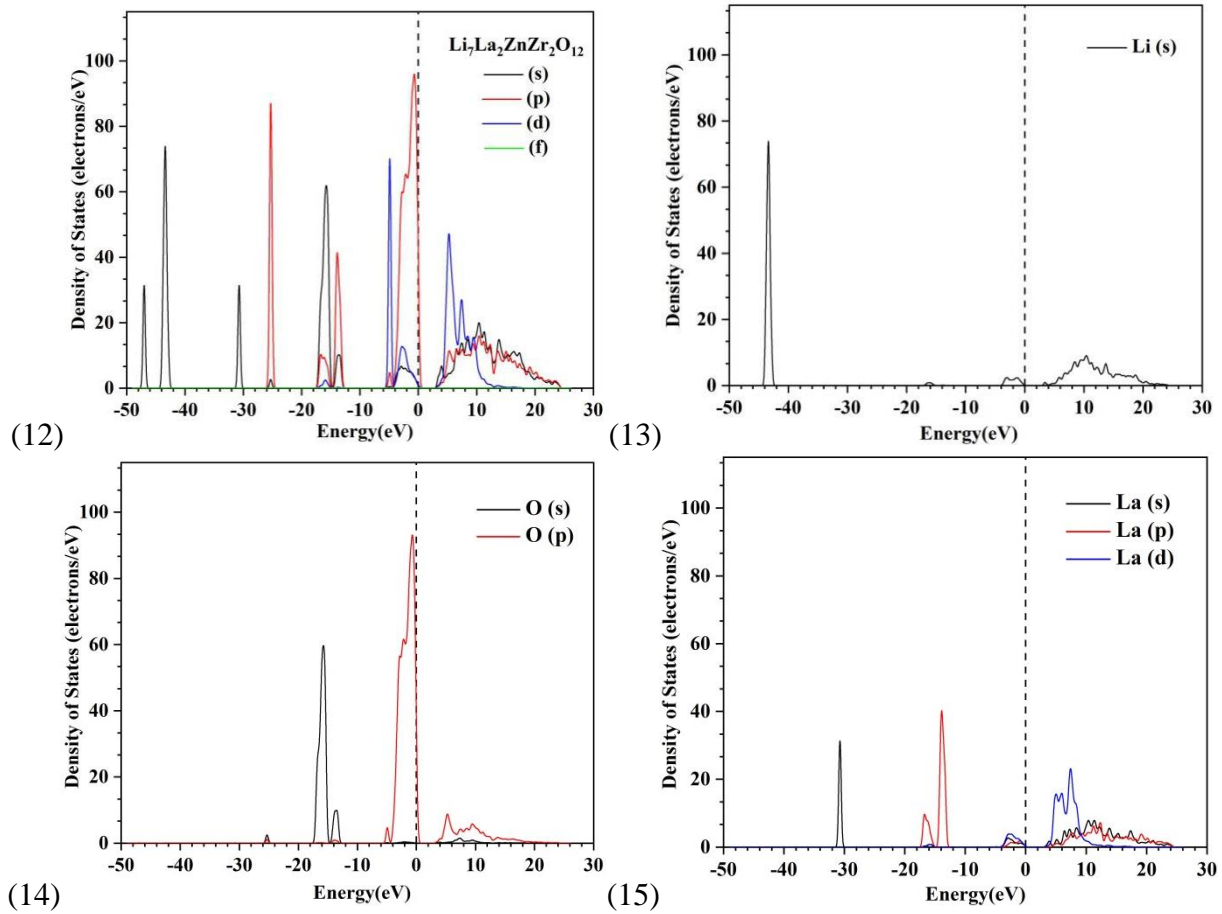


Figure 5. $\text{Li}_6\text{ZnLa}_3\text{Zr}_2\text{O}_{12}$ and the density of states of each atom



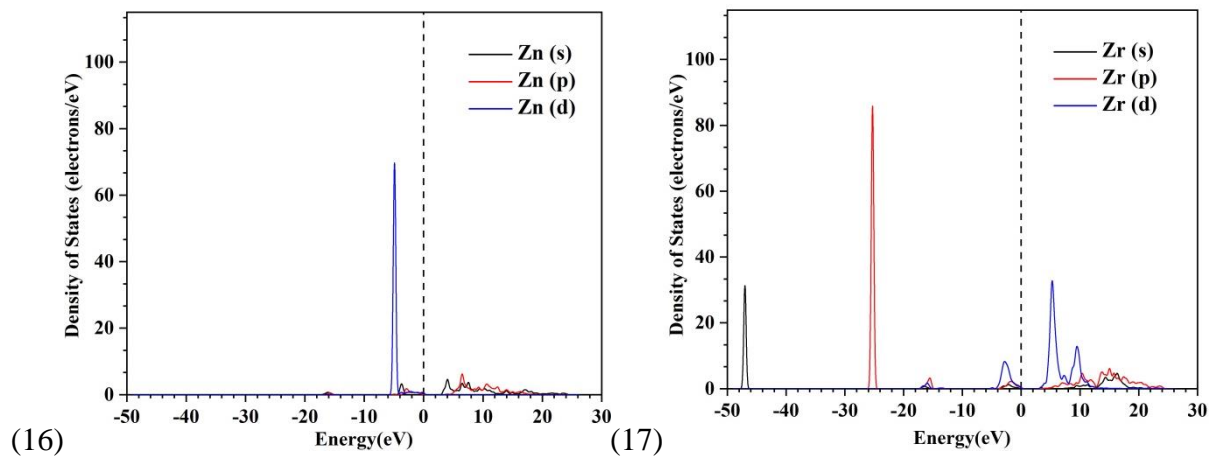


Figure 6. $\text{Li}_7\text{La}_2\text{ZnZr}_2\text{O}_{12}$ and the density of states of each atom

3.3 Population analysis

Population analysis is divided into atomic population analysis and bond population analysis. The distribution of electrons in different atomic orbitals is different, and the bonding of each atom can be obtained by population analysis. The high population value indicates that the bond is covalent, and the low population value indicates that the bond is ionic. The atomic population analysis before and after doping is shown in Table 4, and the bond population analysis in LLZO system before and after doping is shown in Table 5. The bond length is shown in Table 6.

As can be seen from Table 4, the net charge of Li in the LLZO system is 0.95, which is close to the theoretical value 1.00 reported in reference [35], indicating that it has a high degree of ionization and can be embedded and desorbed in the framework formed by Zr-O and La-O. However, the net charges of O, La, and Zr are far from the theoretical charge values, which indicates that the covalent bonds formed by La, Zr, and O are larger than the ionic bonds, and have stronger covalent properties. It also further reflects the characteristics of good stability of tetragonal phase structure [4, 5]. With the doping of Zn, the s-orbital population of Li increases and the net charge decreases, indicating that the contribution of Li ions to the system charge decreases and the interaction with some atoms decreases. The increased net charge of La and Zr indicates that the interaction with O ions is enhanced and the structural stability is improved. In addition, part of the electrons of Zn occupying O formed Zn-O bonds, which reduced the net charge number of O, and the net charge number of Zn doped at La site was greater than that of Li site, indicating that the hole carriers on the covalent bond formed were more. The electrical conductivity is significantly improved, and the electrical conductivity is also increased. It is consistent with the aforementioned analysis.

Table 4. Atomic population (e) of undoped and doped systems

| Ion | Orbit and net charge | LLZO | $\text{Li}_6\text{ZnLa}_3\text{Zr}_2\text{O}_{12}$ | $\text{Li}_7\text{La}_2\text{ZnZr}_2\text{O}_{12}$ |
|-----|----------------------|-------|--|--|
| Li | s | 2.05 | 2.07 | 2.08 |
| | Charge | 0.95 | 0.93 | 0.92 |
| O | s | 1.87 | 1.86 | 1.87 |
| | p | 5.05 | 5.03 | 5.04 |
| | Charge | -0.93 | -0.90 | -0.91 |

| | | | | |
|----|--------|------|------|------|
| La | s | 2.39 | 2.17 | 2.25 |
| | p | 6.39 | 6.31 | 6.35 |
| | d | 1.29 | 1.43 | 1.30 |
| | Charge | 0.92 | 1.08 | 1.10 |
| Zr | s | 2.40 | 2.39 | 2.39 |
| | p | 6.67 | 6.63 | 6.64 |
| | d | 2.09 | 2.07 | 2.08 |
| | Charge | 0.83 | 0.9 | 0.89 |
| Zn | s | - | 0.85 | 0.80 |
| | p | - | 1.08 | 0.78 |
| | d | - | 9.96 | 9.97 |
| | Charge | - | 0.11 | 0.46 |

From Table 5 to 6, it can be seen that doping leads to the increase of Li-O bond population, the decrease of bond length and the enhancement of bond covalent, among which the bond length of $\text{Li}_6\text{ZnLa}_3\text{Zr}_2\text{O}_{12}$ is the smallest, indicating that the Li-O bond covalent is strong in this system. Although it is different from the elements doped with [36], such as Johannes, the change trend of the results is the same. When the Li site is doped, the La-O bond population decreases, the bond length increases, the Zr-O bond population increases, and the bond length decreases, indicating that the covalency of La-O bond weakens, while that of Zr-O bond increases. The opposite is true when La site is doped. This is because the Zn doping at different positions results in different structural changes, the covalentness of some bonds is enhanced or weakened, and new Zn-O bonds are generated to enhance the stability of the structure. However, the population of Zn-O bonds in $\text{Li}_6\text{ZnLa}_3\text{Zr}_2\text{O}_{12}$ is much larger than that of $\text{Li}_7\text{La}_2\text{ZnZr}_2\text{O}_{12}$ system, and the minimum bond length is 1.9475\AA , indicating that the covalent nature of the bonds is strong and the stability is better. The results show that because of the smaller Coulomb repulsion force between the adjacent $[\text{LiO}_4]$ tetrahedron and $[\text{LiO}_6]$ octahedron Li^+ - Li^+ , the Li^+ occupancy rate is higher and the electrical conductivity is lower in the LLZO tetragonal structure [6, 33]. It was found through doping that the Li-Li bond length decreased and the Coulomb repulsion force between Li^+ - Li^+ increased, which was beneficial to increase the Li vacancy concentration and thus improve the conductivity. Although the Li-Li bond length of $\text{Li}_6\text{ZnLa}_3\text{Zr}_2\text{O}_{12}$ system is the smallest, it has an effect on the electrical conductivity due to the high doping concentration of Zn. Therefore, the concentration of doping elements is not the greater the more advantageous.

Table 5. Bond population average of Zn-doped crystals (e)

| Bond | LLZO | $\text{Li}_6\text{ZnLa}_3\text{Zr}_2\text{O}_{12}$ | $\text{Li}_7\text{La}_2\text{ZnZr}_2\text{O}_{12}$ |
|-------|-------|--|--|
| Li-Li | 0.123 | 0.227 | 0.070 |
| Li-O | 0.010 | 0.027 | 0.015 |
| La-O | 0.285 | 0.233 | 0.287 |
| Zr-O | 0.523 | 0.526 | 0.477 |
| Zn-O | - | 0.520 | 0.040 |

Table 6. Average bond length of Zn-doped crystals (Å)

| Model | Li-Li | Li-O | La-O | Zr-O | Zn-O |
|---|-------|-------|-------|-------|-------|
| LLZO | 2.647 | 2.293 | 2.601 | 2.124 | - |
| Li ₆ ZnLa ₃ Zr ₂ O ₁₂ | 2.560 | 2.156 | 2.645 | 2.122 | 1.947 |
| Li ₇ La ₃ ZnZr ₂ O ₁₂ | 2.620 | 2.273 | 2.584 | 2.128 | 2.968 |

4. CONCLUSIONS

1) Through the structure analysis, it is found that the structure of Zn-doped LLZO system is more stable, and the total energy of Li site doping is -53104eV, which is more stable.

2) Analysis of energy bands and band density shows that the number of energy bands near the Fermi level increases and the band gap decreases from 9.6eV to 3.81eV (Li) and 3eV (La) due to the action of Zn electrons in different orbits, which is beneficial to electrons or air Jump of the cave. The energy required for the electron or hole transition is reduced, the electrical conductivity is increased, and the electrical conductivity of the La-site doping is relatively high.

3) Population analysis shows that different positions of Zn doping improve the covalent nature of Zr-O and La-O bonds, and generate Zn-O bonds, which is beneficial to improve the structural stability. The bond length of Zn-O in Li₆ZnLa₃Zr₂O₁₂ system is 1.9475Å, which is more covalent than that of Li₇La₃ZnZr₂O₁₂. Moreover, when the bond length of Li-Li decreases, the Coulomb repulsion force between Li⁺-Li⁺ increases, which is beneficial to increase the vacancy concentration of Li and increase the electrical conductivity.

4) Although doping can improve stability and conductivity, both are affected by the doping concentration. If the doping amount is too large, it will not be conducive to improving the conductivity.

ACKNOWLEDGEMENTS

This work was supported by Fund Project of Guangxi Key Laboratory of Automobile Components and Vehicle Technology, Guangxi University of Science and Technology (No.2017GKLACVTZZ04). Innovation Project of Guangxi University of Science and Technology Graduate Education (YCSW2020217). GDAS' Special Project of Science and Technology Development, Guangdong Academy of Science (N0.2017GDAS CX-0202). Innovation Team Project of Guangxi University of Science and Technology (No.3). Fund Project of the Key Lab of Guangdong for Modern Surface Engineering Technology (No.2018KFKT01). What's more, thank you for the theoretical support of Shenzhen Cloud Computing Center.

References

1. Y. M. He, C. Y. Lu, S. Liu, W. J. Zheng and J. Y. Luo, *Adv. Energy Mater.*, 9 (2019) 1901810.
2. R. Murugan, V. Thangadurai and W. Weppner, *Angew. Chem. Int. Ed.*, 46 (2007) 7778.
3. V. Thangadurai, H. Kaack and W. J. F. Weppner, *J. Am. Ceram. Soc.*, 86 (2003) 437.
4. R. Jalem, M. J. D. Rushton, W. J. Manalastas, M. Nakayama, T. Kasuga, J. A. Kilner and R. W.

- Grimes, *Chem. Mater.*, 27 (2015) 2821.
5. L. Dhivya, N. Janani, B. Palanivel and R. Murugan, *AIP Adv.*, 3 (2013) 082115.
 6. K. Meier, T. Laino and A. Curioni, *J. Phys. Chem. C*, 118 (2014) 6668.
 7. K. C. Santosh, R. C. Longo, K. Xiong and K. Cho, *Solid State Ionics*, 261 (2014) 100.
 8. N. Bernstein, M. D. Johannes and K. Hoang, *Phys. Rev. Lett.*, 109 (2012) 205702.
 9. S. Adams and P. Raor, *J. Mater. Chem.*, 22 (2012) 1426.
 10. Y. Li, J. T. Han, C. A. Wang, H. Xie and J. B. Goodenough, *J. Mater. Chem.*, 22 (2012) 15357.
 11. M. Xu, M. S. Park, J. M. Lee, T. Y. Kim and Y. S. Park, *Phys. Rev. B*, 85 (2012) 052301.
 12. Y. X. Wang, M. Klenk, K. Page and W. Lai, *Chem. Mater.*, 26 (2014) 5613.
 13. C. A. Geiger, E. Alekseev, B. Lazic, M. Fisch, T. Armbruster, R. Langner, M. Fechtelkord, N. Kim, T. Pettke and W. Weppner, *Inorg. Chem.*, 50 (2011) 1089.
 14. D. Rettenwander, P. Blaha, R. Laskowski, K. Schwarz, P. Bottke, M. Wilkening, C. A. Geiger and G. Amthauer, *Chem. Mater.*, 26 (2014) 2617.
 15. L. J. Miara, S. P. Ong, Y. Mo, W. D. Richards, Y. Park, J. M. Lee, H. S. Lee and G. Ceder, *Chem. Mater.*, 25 (2013) 3048.
 16. G. Z. Li, *H. I. T.*, (2017).
 17. S. Ohta, T. Kobayashi and T. Asaoka, *J. Power Sources*, 196 (2011) 3342.
 18. N. Janani, S. Ramakumar, S. Kannan and R. Murugan, *J. Am. Ceram. Soc.*, 98 (2015) 2039.
 19. R. Murugan, S. Ramakumar and N. Janani, *Electrochem. Commun.*, 13 (2011) 1373.
 20. S. Ramakumar, L. Satyanarayana, S. V. Manorama and R. Murugan, *Phys. Chem. Chem. Phys.*, 15 (2013) 11327.
 21. Y. Wang and W. Lai, *Electrochem. Solid. ST*, 15 (2012) A68.
 22. E. Rangasamy, J. Wolfenstine, J. Allen and J. Sakamoto, *J. Power Sources*, 230 (2013) 261.
 23. K. Masashi, M. Hirokazu and K. Kiyoshi, *J. Electrochem. Soc.*, 157 (2010) 1076.
 24. R. Inada, K. Kusakabe, T. Tanaka, S. Kudo and Y. Sakurai, *Solid State Ionics*, 262 (2014) 568.
 25. J. Awaka, N. Kijima, H. Hayakawa and J. Akimoto, *J. Solid State Chem.*, 182 (2009) 2046.
 26. F. Langer, J. Glenneberg, I. Bardenhagen and R. Kun, *J. Alloys Compd.*, 645 (2015) 64.
 27. E. Y. Yi, W. M. Wang, J. Kieffer and R. M. Laine, *J. Power Sources*, 352 (2016) 156.
 28. S. Ohta, T. Kobayashi, J. Seki and T. Asaoka, *J. Power Sources*, 202 (2012) 332.
 29. L. J. Miara, W. D. Richards, Y. E. Wang and G. Ceder, *Chem. Mater.*, 27 (2015) 4040.
 30. T. Yang, G. D. Gordon, Y. Li and C. K. Chan, *J. Phys. Chem. C*, 119 (2015) 14947.
 31. V. Thangadurai, D. Pinzaru, S. Narayanan and A. K. Baral, *J. Phys. Chem. Lett.*, 6 (2015) 292.
 32. C. Deviannapoorani, L. Dhivya, S. Ramakumar and R. Murugan, *J. Power Sources*, 240 (2013) 18.
 33. J. F. Wu, E. Y. Chen, Y. Yao, Y. Wu, W. K. Pang, V. K. Peterson and X. Guo, *ACS Appl. Mater. Interfaces*, 9 (2016) 1542.
 34. F. Du, N. Zhao, Y. Li, C. Chen, Z. Liu and X. Guo, *J. Power Sources*, 300 (2015) 24.
 35. J. Awaka, A. Takashima, K. Kataoka, N. Kijima, Y. Idemoto and J. Akimoto, *Chem. Lett.*, 40 (2011) 60.
 36. S. Mukhopadhyay, T. Thompson, J. Sakamoto, A. Huq, J. Wolfenstine, J. Allen, N. Bernstein, D. A. D. A. Stewart and M. D. Johannes, *Chem. Mater.*, 27 (2015) 3658.